A Comparison of Open-Loop Suppressed-Carrier Acquisition Techniques

B. Shah
Radio Frequency and Microwave Subsystems Section

S. Hinedi
Communications Systems Research Section

This article compares three open-loop suppressed-carrier acquisition techniques that are being considered for the Advanced Receiver II (ARX II). The algorithms (full-, half-, and staggered-symbol integration) employ fast Fourier transforms (FFTs) to detect the carrier-frequency offset in the presence of symbol-timing errors. Expressions for the detection probability of the frequency offset as a function of both the symbol signal-to-noise ratio (SNR) and constant symbol-timing errors are derived, and it is shown that the staggered-symbol integration technique has the best performance at low received symbol SNR, making it the preferred implementation for Deep Space Network applications.

I. Introduction

The Advanced Receiver II (ARX II) [1] uses a digital Costas loop to demodulate binary phase shift keyed (BPSK) signals in the absence of residual carrier. Typically, frequency acquisition begins by tuning the Costas loop's numerically controlled oscillator (NCO) to a predicted received frequency. If the frequency difference Δf between the received and predicted frequency is on the order of the one-sided Costas (closed) loop bandwidth B_L, the frequency error is within the pull-in range of the loop, and acquisition is easily achieved. However, if the frequency error is outside the pull-in range of the loop, some form of frequency aiding, which has to be accomplished in the absence of symbol synchronization, is necessary to facilitate acquisition. One such technique is to sweep the NCO at a sufficiently low rate so as to enable the loop to lock up. While sweeping can be accomplished with either a matched or a lowpass filter in the loop arms, the latter does not require symbol synchronization but is suboptimum. As an example, when the 3-dB bandwidth of the arm filter (assuming a first-order Butterworth filter) is

equal to the data rate, the degradation in loop signal-to-noise ratio (SNR) is about 2.1 dB and 1.1 dB, when the received symbol SNR is −3 dB and 3 dB, respectively [2].

The techniques investigated in this article perform fast Fourier transforms (FFTs) on the phase-detector output of Costas-type loops, which employ integrate-and-dump filters. The timing signal controlling these filters is kept constant (at the predicted symbol rate) by "opening up" the symbol-synchronization loop. It is assumed that the symbol rate, but not necessarily the symbol epoch, is known precisely. In that case, the integrators operate with a symbol-timing offset τ, which is some unknown but fixed fraction of the symbol interval T. The three open-loop techniques, depicted in Figs. 1, 2, and 3, detect the carrier by searching the magnitude spectrum of the error signal $Z(n)$ for a tone at $2\Delta f$ Hz, since an error Δf at the integrator inputs yields an error $2\Delta f$ at the input to the FFT. The spectrum is a function of many variables, including the symbol-timing offset τ. Expressions for the detection and outlier probabilities are derived for all the schemes as a function of symbol SNR, symbol rate, FFT size, and timing offset τ.

The full-symbol scheme, depicted in Fig. 1, is considered because it is the easiest to implement. The ARX II uses a Costas loop to track BPSK signals. Consequently, the full-symbol integration technique can be implemented by simply "opening up" the Costas loop. That is, instead of feeding back the loop error signal to reduce the frequency error Δf, the signal is accumulated and fast Fourier transformed to obtain the error signal magnitude spectrum.

One disadvantage of the full-symbol integration technique is its worsened performance when the symbol-timing offset τ is close to half a symbol period. In this case, the integrator integrates across symbol boundaries and, as a result, the full-symbol error signal, $Z_f(n)$ in Fig. 1, is noise alone half the time (assuming that the probability of symbol transition is one-half). This disadvantage motivates the consideration of the half-symbol technique of Fig. 2, in which the integration window is halved. As a result, integrations across symbol boundaries occur only half as often as the full-symbol case. Consequently, the error signal is noise alone a quarter of the time, an improvement over the full-symbol case. However, for small timing offsets, the half-symbol error signal is degraded when compared with the full-symbol error signal, because the full-symbol technique approaches a matched filter (for non-return-to-zero [NRZ] pulses) but the half-symbol technique does not. As a compromise between the two schemes, consider the staggered-symbol integration technique in Fig. 3. This scheme uses two full-symbol integrator channels, with the top channel delayed by half a symbol with respect to the bottom channel. The advantage here is that the staggered-symbol error signal $Z_s(n)$ is never noise alone, because if the integrators in one channel straddle symbol boundaries, the other channel is synchronous with the symbol epochs. As a result, the composite error signal, which is the sum of the delayed and undelayed error signals, always has signal plus noise. The disadvantage of this scheme is that it requires more hardware and suffers from self-noise, as will be shown. However, the self-noise is significant only at high symbol SNRs, an unimportant region to the Deep Space Network (DSN).

A mathematical model for these techniques is derived in Section II; their performance in terms of the probability of detecting the frequency difference between the received and predicted frequency is given in Section III. Concluding remarks are in Section IV.

II. Mathematical Model

The received suppressed-carrier BPSK signal, downconverted to an appropriate intermediate frequency (IF), can be modeled as

$$r(t) = \sqrt{2P}d(t)\sin(\omega_i t + \theta_i) + n(t) \tag{1}$$

where P is the received power in watts, ω_i is the IF radian frequency in rad/sec, θ_i is the signal phase in rad, and $d(t)$ is the transmitted data stream given by

$$d(t) = \sum_{k=-\infty}^{+\infty} d_k p(t - kT) \tag{2}$$

where $p(t)$ is the baseband NRZ pulse limited to T sec, and d_k is the term for the equally likely ± 1 binary symbols. The narrow-band noise process $n(t)$ can be expressed as

$$n(t) = \sqrt{2}n_c(t)\cos(\omega_i t + \theta_i) - \sqrt{2}n_s(t)\sin(\omega_i t + \theta_i) \tag{3}$$

where $n_c(t)$ and $n_s(t)$ are statistically independent, stationary, band-limited white Gaussian noise processes with one-sided spectral density N_0 W/Hz and one-sided bandwidth, W Hz. The signal $r(t)$ is demodulated by in-phase and quadrature references $\sqrt{2}\sin(\omega_0 t + \theta_0)$ and $\sqrt{2}\cos(\omega_0 t + \theta_0)$ before being integrated over a half or full symbol, depending on the technique being implemented. Then, the integrator outputs are multiplied to produce the various error signals $Z_f(n)$, $Z_h(n)$, and $Z_s(n)$. Steps

detailing the derivation of the error signals for full-, half-, and staggered-symbol cases are in Appendices A, B, and C, respectively. In each case, the error signal is a sinusoid in white noise with frequency $2\Delta f$ Hz ($\Delta f = (\omega_0 - \omega_i)/2\pi$) and amplitude $A(P, \tau)$, which is a function of the received signal power and symbol-timing offset. Consequently, the absolute frequency difference $|\Delta f|$ can be detected by observing the magnitude of the frequency spectrum of the appropriate error signal. Only the absolute value of Δf can be detected because of the real FFT operation. Note that the sign ambiguity problem can be resolved by offsetting the frequency so that the error Δf always has a known sign. The probability of detection P_D of a tone in white Gaussian noise is well known [3] and can be easily computed as a function of the error signal SNR. The key results of [3] are repeated in Appendix D for the reader's convenience. The strategy here is to express the error signal of each technique in the same form as Eq. (D-1) and then apply the results of Appendix D in a straightforward manner.

A. Full-Symbol Integration

A detailed analysis of the full-symbol integration technique is contained in Appendix A; the main results of the analysis are shown below. Assuming the double-frequency terms of the demodulated signals $I(t)$ and $Q(t)$ in Fig. 1 are fast-varying with respect to the symbol rate R_s, and the difference terms at $\Delta f \triangleq f_i - f_o$ vary slowly compared to R_s, the inphase and quadraphase arm outputs $Z_{f,i}(n)$ and $Z_{f,q}(n)$ are approximately given as

$$Z_{f,i}(n) = \sqrt{P} D_f(n) \cos\big(\Delta\omega(nT + T/2 + \tau T) + \phi\big) + N_{f,i}(n) \tag{4}$$

$$Z_{f,q}(n) = \sqrt{P} D_f(n) \sin\big(\Delta\omega(nT + T/2 + \tau T) + \phi\big) + N_{f,q}(n) \tag{5}$$

where $\phi \triangleq \theta_i - \theta_0$ is the phase error, $D_f(n)$ is the integral of $d(t)$ over the T-sec interval, $[(n+\tau)T, (n+1+\tau)T]$; and the integrals of $\sin(\Delta\omega t + \phi)$ and $\cos(\Delta\omega t + \phi)$ are approximated by the sinusoids evaluated at the interval midpoint. The term $D_f(n)$ is expressed mathematically as

$$D_f(n) = (1 - \tau) d_n + \tau d_{n+1} \tag{6}$$

where τ is a fraction of the symbol interval T. Note that when $\tau = 1/2$, symbol transitions occur in the middle of the integration interval, and $D_f(n) = 0$ half of the time (assuming symbol transitions occur with probability one-half). The noise samples $N_{f,i}(n)$ and $N_{f,q}(n)$ are given in Appendix A and are shown to be zero mean, independent, Gaussian random variables with variance

$$\sigma_{f,i}^2 = \sigma_{f,q}^2 = N_0/2T \triangleq \sigma^2 \tag{7}$$

The error signal $Z_f(n)$ is formed by taking the product $Z_{f,i}(n) Z_{f,q}(n)$. From Appendix A, one has

$$Z_f(n) = A_f(P, \tau) \sin\big(2\Delta\omega nT + 2\theta_f(\phi)\big) + n_f(n) \tag{8}$$

where

$$A_f(P, \tau) = \frac{P}{2}(1 - 2\tau + 2\tau^2) \tag{9}$$

and $\theta_f(\phi)$ is given by Eq. (A-6). Since the interest here is in the magnitude spectrum of the error signal, the phase $\theta_f(\phi)$ is not utilized but is included in Appendix A for completeness. The effective noise $n_f(n)$ is defined as

$$n_f(n) \triangleq n_{f,ss}(n) + n_{f,sn}(n) + n_{f,nn}(n) \tag{10}$$

where $n_{f,ss}(n)$ is the self-noise due to the signal–signal product, $n_{f,sn}(n)$ is the noise due to the signal–noise product, and $n_{f,nn}(n)$ is the noise–noise term. These noises, given by Eqs. (A-7) through (A-9), are independent with respect to each other and white. Consequently, $n_f(n)$ is white, with variance

$$\sigma_f^2 = \sigma_{f,ss}^2 + \sigma_{f,sn}^2 + \sigma_{f,nn}^2 \tag{11}$$

where

$$\sigma_{f,ss}^2 = \frac{P^2}{2}(1 - \tau)^2 \tau^2 \tag{12}$$

$$\sigma_{f,sn}^2 = P(1 - 2\tau + 2\tau^2)\sigma^2 \tag{13}$$

$$\sigma_{f,nn}^2 = \sigma^4 \tag{14}$$

where σ^2 is given by Eq. (7). In deriving Eqs. (12)–(14), it was assumed that τ and $\Delta\omega$ in Eqs. (A-7) through (A-9) are unknown constants. Furthermore, d_n, $N_{f,i}(n)$, $N_{f,q}(n)$, and ϕ are assumed to be independent random variables, where $\mathcal{E}[d_n] = 0$, $\mathcal{E}[d_n d_m] = \delta_k(n - m)$, and ϕ is uniformly distributed between $[0, 2\pi]$. The term $\mathcal{E}[\cdot]$ is the expectation, and the Kronecker delta

function $\delta_k(n-m)$ is one when $n=m$ and zero otherwise.

Notice that when $\Delta\omega = 0$ and $\tau = 0$, Eq. (8) reduces to the familiar Costas loop tracking-error signal $(P/2)\sin 2\phi + n_f(n)$ [4], where, from Eqs. (12)-(14), $n_f(n)$ has variance $P\sigma^2 + \sigma^4$, as expected. Note also that the self-noise term is zero when $\tau = 0$ or $\tau = 1$, as expected. The signal-to-noise ratio of the sequence $Z_f(n)$, defined as signal power divided by the noise power, is given by

$$SNR_f(\tau) = \frac{A_f^2(P,\tau)}{2\sigma_f^2} = \frac{(1-2\tau+2\tau^2)^2}{4(1-\tau)^2\tau^2 + (1-2\tau+2\tau^2)(4/SNR) + (2/SNR^2)} \tag{15}$$

where $SNR \triangleq PT/N_0$ is the received symbol signal-to-noise ratio. For $\tau = 0$, Eq. (15) simplifies to

$$SNR_f(0) = \frac{SNR}{4 + 2/SNR} \tag{16}$$

B. Half-Symbol Integration

The half-symbol integration technique, shown in Fig. 2, is similar to the full-symbol integration technique, with the inphase and quadraphase integrators now integrating over the $T/2$-sec interval, $[(n+2\tau)T/2, (n+1+2\tau)T/2]$, where τ is a fraction of $T/2$ sec. Breaking up the integration over a symbol into two halves results in symbol transition boundaries occurring in the middle of every other integration interval; as a result, they occur half as many times as in the full-symbol case. One intuitively expects worst-case performance (with the transition boundary in the middle of the integration interval) in the half-symbol case to be better than the full-symbol case. However, when there is perfect symbol timing, half-symbol integration is expected to perform worse than full-symbol integration.

Following similar steps as in Eqs. (4) and (5), the following approximate expressions are obtained for $Z_{h,i}(n)$ and $Z_{h,q}(n)$:

$$Z_{h,i}(n) = \sqrt{P}D_h(n)\cos\big(\Delta\omega(nT/2 + T/4 + \tau T) + \phi\big) + N_{h,i}(n) \tag{17}$$

$$Z_{h,q}(n) = \sqrt{P}D_h(n)\sin\big(\Delta\omega(nT/2 + T/4 + \tau T) + \phi\big) + N_{h,q}(n) \tag{18}$$

where $D_h(n)$ is the integral of $d(t)$ over the $T/2$-sec interval, $[(n+2\tau)T/2,\ (n+1+2\tau)T/2]$. Hence,

$$D_h(n) = \begin{cases} d_{\frac{n}{2}}, & n \text{ even} \\ (1-2\tau)d_{\frac{n-1}{2}} + 2\tau d_{\frac{n+1}{2}}, & n \text{ odd} \end{cases} \tag{19}$$

where even n's represent the integration over the half of a symbol without transitions and odd n's represent the integration over the half with transitions. Notice that in the worst case, where $\tau = 1/4$, $D_h(n) = 0$ a quarter of the time. The terms $N_{h,i}(n)$ and $N_{h,q}(n)$ in Eqs. (17) and (18) can also be expressed as in Eqs. (A-1) and (A-2) with T replaced by $T/2$ and τ replaced by 2τ. Consequently, $N_{h,i}(n)$ and $N_{h,q}(n)$ are zero mean, independent, Gaussian random variables with variance

$$\sigma_{h,i}^2 = \sigma_{h,q}^2 = N_0/T = 2\sigma^2 \tag{20}$$

As shown in Fig. 2, the half-symbol error signal is formed by summing two consecutive samples of the product $Z_{h,i}(n)Z_{h,q}(n)$. From Eq. (B-8), $Z_h(n)$ is given as

$$Z_h(n) = A_h(P,\tau)\sin\big(2\Delta\omega nT + 2\theta_h(\phi)\big) + n_h(n) \tag{21}$$

where

$$A_h(P,\tau) = \frac{P}{2}(1-2\tau+4\tau^2) \tag{22}$$

and $\theta_h(\phi)$ is given by Eq. (B-11). The effective noise in Eq. (21) is

$$n_h(n) \triangleq n_{h,ss}(n) + n_{h,sn}(n) + n_{h,nn}(n) \tag{23}$$

where $n_{h,ss}(n)$, $n_{h,sn}(n)$, and $n_{h,nn}(n)$ as given by Eqs. (B-12) through (B-14) are independent and white. As a result, $n_h(n)$ is also white, with variance

$$\sigma_h^2 = \sigma_{h,ss}^2 + \sigma_{h,sn}^2 + \sigma_{h,nn}^2 \tag{24}$$

where

$$\sigma^2_{h,ss} = \frac{P^2}{2}(1-2\tau)^2\tau^2 \tag{25}$$

$$\sigma^2_{h,sn} = P(1-2\tau+4\tau^2)\sigma^2 \tag{26}$$

$$\sigma^2_{h,nn} = 2\sigma^4 \tag{27}$$

Note that when tracking with perfect symbol timing (i.e., $\Delta\omega = 0$ and $\tau = 0$), the half-symbol error signal reduces to $(P/2)\sin 2\phi$ plus noise, with variance $P\sigma^2+2\sigma^4$ as expected. The signal-to-noise ratio of $Z_h(n)$ is given by

$$SNR_h(\tau) = \frac{(1-2\tau+4\tau^2)^2}{4(1-2\tau)^2\tau^2+(1-2\tau+4\tau^2)(4/SNR)+(4/SNR^2)} \tag{28}$$

which, when $\tau = 0$, reduces to

$$SNR_h(0) = \frac{SNR}{4+4/SNR} \tag{29}$$

Note that at high symbol SNRs (i.e., ignoring squaring losses), $SNR_h(0)$ and $SNR_f(0)$ are equal because of the accumulation over two half-symbols in Fig. 2.

C. Staggered-Symbol Integration

Staggered-symbol integration has two full-symbol integrator channels, with one channel delayed by half a symbol with respect to the symbol-transition boundary. Unlike the full- and half-symbol integration techniques, the signal component of the staggered-symbol error signal $Z_s(n)$, which is the sum of the delayed and undelayed error signals $Z_d(n)$ and $Z_u(n)$, is always nonzero. For example, when there is perfect symbol timing, the undelayed channel never integrates across symbol-transition boundaries and the delayed channel always does. As a result, $Z_u(n)$ always has a nonzero signal portion, whereas the signal part of $Z_d(n)$ is zero half the time. When symbol timing is off by half a symbol, the delayed channel-integration intervals are synchronous with transition boundaries and the error signal scenario is reversed. In view of the two scenarios described above, identical performance is expected when symbol timing is perfect or off by half a symbol. Exact expressions for the error signals are derived in Appendix C and also shown below. The undelayed channel in Fig. 3 is the same as the full-symbol integration shown in Fig. 1. Hence, $Z_u(n)$ in Fig. 3 is identical to the full-symbol error signal $Z_f(n)$ given by Eq. (8). The delayed channel integrates the demodulated signal over the T-sec interval, $[(n+\frac{1}{2}+\tau)T, (n+\frac{3}{2}+\tau T]$. Consequently, the delayed inphase and quadraphase integrator outputs have the same form as the undelayed outputs given by Eqs. (4) and (5), namely

$$Z_{d,i}(n) = \sqrt{P}D_d(n)\cos\big(\Delta\omega(nT+T+\tau T)+\phi\big) + N_{d,i}(n) \tag{30}$$

$$Z_{d,q}(n) = \sqrt{P}D_d(n)\sin\big(\Delta\omega(nT+T+\tau T)+\phi\big) + N_{d,q}(n) \tag{31}$$

where $D_d(n)$ is the integral of $d(t)$ over the delayed interval, and the integral of $\sin(\Delta\omega t+\phi)$ and $\cos(\Delta\omega t+\phi)$ over the same interval is approximated by the sinusoid evaluated at the interval midpoint. The quantity $D_d(n)$ is expressed mathematically as

$$D_d(n) = \left(\frac{1}{2}-\tau\right)d_n + \left(\frac{1}{2}+\tau\right)d_{n+1} \tag{32}$$

where τ is a fraction of $T/2$ sec. The noises $N_{d,i}(n)$ and $N_{d,q}(n)$ are given by Eqs. (A-1) and (A-2), with the limits of integration changed to that of the delayed case. From Eq. (C-1), one has

$$Z_d(n) = A_d(P,\tau)\sin\big(2\Delta\omega nT + 2\theta_d(\phi)\big) + n_d(n) \tag{33}$$

where the amplitude of $Z_d(n)$ is given by

$$A_d(P,\tau) = \frac{P}{2}\left(\frac{1}{4}-\tau^2\right) \tag{34}$$

and the phase $\theta_d(\phi)$ is defined by Eq. (C-4). The effective noise $n_d(n)$ is given by

$$n_d(n) \triangleq n_{d,ss}(n) + n_{d,sn}(n) + n_{d,nn}(n) \tag{35}$$

where $n_{d,ss}(n)$ and $n_{d,sn}(n)$ given by Eqs. (C-5) through (C-7) are uncorrelated and white. Consequently, $n_d(n)$ is white, with variance

$$\sigma^2_d = \sigma^2_{d,ss} + \sigma^2_{d,sn} + \sigma^2_{d,nn} \tag{36}$$

where

$$\sigma^2_{d,ss} = \frac{P^2}{2}\left(\frac{1}{4}-\tau^2\right) \tag{37}$$

$$\sigma^2_{d,sn} = P\left(\frac{1}{2} + 2\tau^2\right)\sigma^2 \tag{38}$$

$$\sigma^2_{d,nn} = \sigma^4 \tag{39}$$

The staggered-symbol integration error signal $Z_s(n)$ is the sum of $Z_u(n) + Z_d(n)$. As shown in Appendix C, it can be written as

$$Z_s(n) = A_s(P,\tau)\sin\left(2\Delta\omega nT + 2\theta_s(\phi)\right) + n_s(n) \tag{40}$$

where the amplitude

$$A_s(P,\tau) = \frac{P}{2}\left(\frac{3}{2} - 2\tau + 4\tau^2\right) \tag{41}$$

and $\theta_s(\phi)$ is given by Eq. (C-12). The effective noise $n_s(n) = n_u(n) + n_d(n)$ is given by Eqs. (C-13) through (C-17). Note that although $n_u(n)$ and $n_d(n)$ are white, $n_s(n)$ is correlated because of the cross-correlation between $n_u(n)$ and $n_d(n)$, due to the half-symbol delay. In particular, $n_{s,sn}$ and $n_{s,nn}$ as given by Eqs. (C-15) and (C-16) are correlated, whereas $n_{s,ss}$ given by Eq. (C-14) is white. From Appendix C, the average power of $n_s(n)$ (average power is denoted by σ^2 for consistency in notation) is given as

$$\sigma^2_s = \sigma^2_{s,ss} + \sigma^2_{s,sn} + \sigma^2_{s,nn} \tag{42}$$

where

$$\sigma^2_{s,ss} = \frac{P^2}{2}\left(\frac{1}{4} + \tau - 2\tau^2\right)^2 \tag{43}$$

$$\sigma^2_{s,sn} = P(2 - 3\tau + 6\tau^2)\sigma^2 \tag{44}$$

$$\sigma^2_{s,nn} = \frac{5}{2}\sigma^4 \tag{45}$$

Note that unlike the previous two techniques, the self-noise is nonzero even when tracking with perfect symbol synchronization. Furthermore, since it increases with signal power, staggered-symbol performance can be expected to worsen with increasing received symbol SNR. The staggered-symbol signal-to-noise ratio is given by

$$SNR_s(\tau) = \frac{(3/2 - 2\tau + 4\tau^2)^2}{4(1/4 + \tau - 2\tau^2)^2 + (2 - 3\tau + 6\tau^2)(4/SNR) + 5/SNR^2} \tag{46}$$

which, when $\tau = 0$, reduces to

$$SNR_s(0) = \frac{9SNR}{SNR + 32 + 20/SNR} \tag{47}$$

III. Numerical Results and Discussion

This section presents curves relating the error signal SNR to the symbol SNR for a fixed τ. The probability of detecting the frequency error $2\Delta f$ is computed, and a numerical example showing how to use the curves is also given.

Figure 4 depicts the SNR degradation (denoted by D) of the different schemes considered versus the timing offset τ. Degradation is defined as the reduction in error signal SNR relative to the SNR of the error signal of a Costas loop with $\tau = 0$. The full-, half-, and staggered-symbol degraded SNRs are given below, where the SNR of the Costas loop error signal $SNR_f(0)$ is given by Eq. (16) and $SNR_f(\tau)$, $SNR_h(\tau)$, and $SNR_s(\tau)$ are given by Eqs. (15), (28), and (46). Therefore

$$D_f(\tau) = \frac{SNR_f(\tau)}{SNR_f(0)}$$

$$= \frac{(2/SNR^2 + 4/SNR)(1 - 2\tau + 2\tau^2)^2}{2/SNR^2 + 4(1-\tau)^2\tau^2 + 4(1 - 2\tau + 2\tau^2)/SNR} \tag{48}$$

$$D_h(\tau) = \frac{SNR_h(\tau)}{SNR_f(0)}$$

$$= \frac{(2/SNR^2 + 4/SNR)(1 - 2\tau + 4\tau^2)^2}{4/SNR^2 + 4(1-2\tau)^2\tau^2 + 4(1 - 2\tau + 4\tau^2)/SNR} \tag{49}$$

$$D_s(\tau) = \frac{SNR_s(\tau)}{SNR_f(0)}$$

$$= \frac{(4/SNR^2 + 8/SNR)(3/2 - 2\tau + 4\tau^2)^2}{5/SNR^2 + 4(1/4 + \tau - 2\tau^2) + 4(2 - 3\tau + 6\tau^2)/SNR} \quad (50)$$

Figure 4 depicts D_f, D_h, and D_s versus τ for various symbol SNRs. Figure 4(a), with SNR = -10 dB, Fig. 4(b), with SNR = -5 dB, and Fig. 4(c), with SNR = 0 dB, indicate that, except for a very small region near $\tau = 0$, the staggered-symbol technique has the best performance for low symbol SNR; Figure 4(d), with SNR = 5 dB, and Fig. 4(e), with SNR = 10 dB, suggest that the half-symbol technique is best for high symbol SNR under a worst-case scenario (i.e., $\tau = 1/4$). The reference SNR, $SNR_f(0)$, is depicted versus symbol SNR in Fig. 5. Figure 5, together with Fig. 4, relate received symbol SNR to error-signal SNR of the various schemes.

Figures 6(a) and 6(b) depict simulation results for the spectrum of the full-symbol error signal $Z_f(n)$ when the frequency offset Δf = 10 Hz, the symbol rate R_s = 1000 Hz, and the symbol SNR = 10 dB for $\tau = 0$, shown in Fig. 6(a), and $\tau = 0.3$, shown in Fig. 6(b). Consistent with the earlier assumption, the frequency offset was chosen to be much smaller than the symbol rate. In both cases, a strong signal component was observed at 20 Hz, indicating a Δf of ± 10 Hz, with the strongest corresponding to the case $\tau = 0$, as expected.

The outlier probability q, defined as the probability that the magnitude of any FFT noise-only bin exceeds the magnitude of the signal-plus-noise bin, is given by $1 - p$, where p is the probability of detecting the real tone and is given by Eq. (D-3). Note that the detection probability given by Eq. (D-3) is based on observing $M/2 + 1$ cells of the magnitude spectrum of an M-point FFT. This is because the FFT operator in Fig. 1 operates on a real input, which results in $M/2 + 1$ distinct cells of the M total cells. Figure 7 depicts q versus SNR where SNR corresponds to the signal-to-noise ratio at the FFT input (i.e., the error signal SNR). Strictly speaking, Fig. 7 applies only when the noise prior to the FFT operation is white and Gaussian. In the case described here, the noise component of the error signal $n_f(n)$, $n_h(n)$, or $n_s(n)$ is not Gaussian, but it is approximated as such because in a hardware implementation the processing rate is reduced from the symbol rate to a more appropiate loop update rate by accumulating over N symbols. As a result, the Gaussian approximation is justified by the Central Limit Theorem for large N. It was shown earlier that $n_f(n)$ and $n_h(n)$ are white, whereas $n_s(n)$ is correlated with its adjacent samples. The curves in Fig. 7 are used for the staggered-symbol case because, for large N, the correlation between adjacent blocks of N samples of $n_s(n)$ will be small enough so that noise samples going in to the FFT operator can be considered to be white.

The following example illustrates how to use the curves presented in this section to compute probability of detection. Suppose that the received symbol SNR is 0 dB. Then, from Fig. 5, the Costas loop error-signal SNR, $SNR_f(0)$, is -11 dB. Assuming that the timing offset $\tau = 0.2$, then, from Fig. 4(c), $D_f(0.2)$, $D_h(0.2)$, and $D_s(0.2)$ are 2.4 dB, 3.1 dB, and 1.3 dB, respectively. As a result, the signal-to-noise ratios of the various error signals $SNR_f(0.2)$, $SNR_h(0.2)$, and $SNR_s(0.2)$ are -13.4 dB, -14.1 dB, and -12.3 dB, respectively. From Fig. 7, the corresponding outlier probabilities for an M = 1024-point FFT are 0.12×10^{-2}, 0.52×10^{-2}, and 0.54×10^{-4} for the full-, half-, and staggered-symbol cases, respectively.

To obtain the outlier probability when τ is not known, the above calculation is performed for all τ, or a reasonable number of τ, and the probabilities are averaged. For instance, when the symbol rate R_s is not known precisely, and the symbol-rate error ΔR_s is small compared to R_s, the symbol rate slips slowly with respect to the integration interval, and τ can be modeled as a uniform random variable. On the other hand, if ΔR_s is not small, then τ can be modeled as a Gaussian random variable. Also note that the results above are limited to the case that $\Delta f << R_s$, and the methods discussed here will not be applicable to the case of low data rates and large frequency errors (i.e., when $\Delta f = R_s$). In the latter case, it may be better to replace the integrators in Figs. 1–3 with lowpass filters.

IV. Conclusion

This article compares three open-loop, suppressed-carrier acquisition techniques (full-, half-, and staggered-symbol integration) which employ FFTs to detect the carrier frequency offset. The staggered-symbol integration technique is shown to have the least degradation at low symbol SNRs, making it the preferred technique for deep-space applications.

Acknowledgment

The authors thank Dr. Jack Holmes for his helpful comments and useful discussions.

References

[1] S. Hinedi, "A Functional Description of the Advanced Receiver," *TDA Progress Report 42-100*, vol. October–December 1989, Jet Propulsion Laboratory, Pasadena, California, pp. 131–149, February 15, 1990.

[2] J. K. Holmes, *Coherent Spread Spectrum Systems*, New York: John Wiley & Sons, 1982.

[3] D. C. Rife and R. R. Boorstyn, "Single-Tone Parameter Estimation from Discrete-Time Observations," *IEEE Trans. Info. Theory*, vol. IT-20, no. 5, pp. 591–598, September 1974.

[4] F. M. Gardner, *Phase Lock Techniques*, 2nd edition, New York: John Wiley & Sons, 1979.

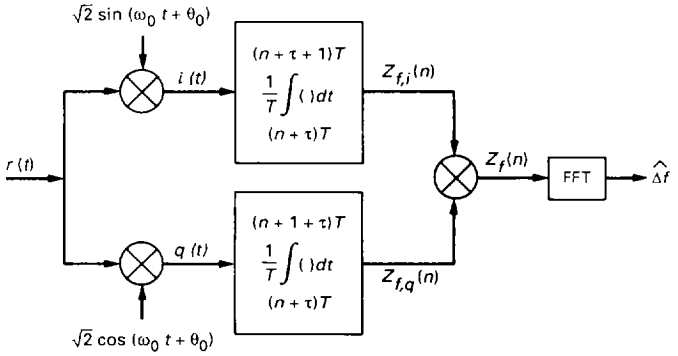

Fig. 1. Full-symbol integration technique.

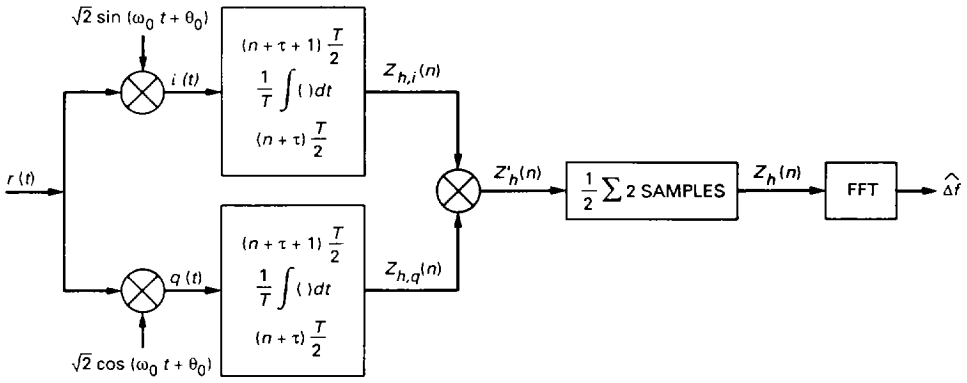

Fig. 2. Half-symbol integration technique.

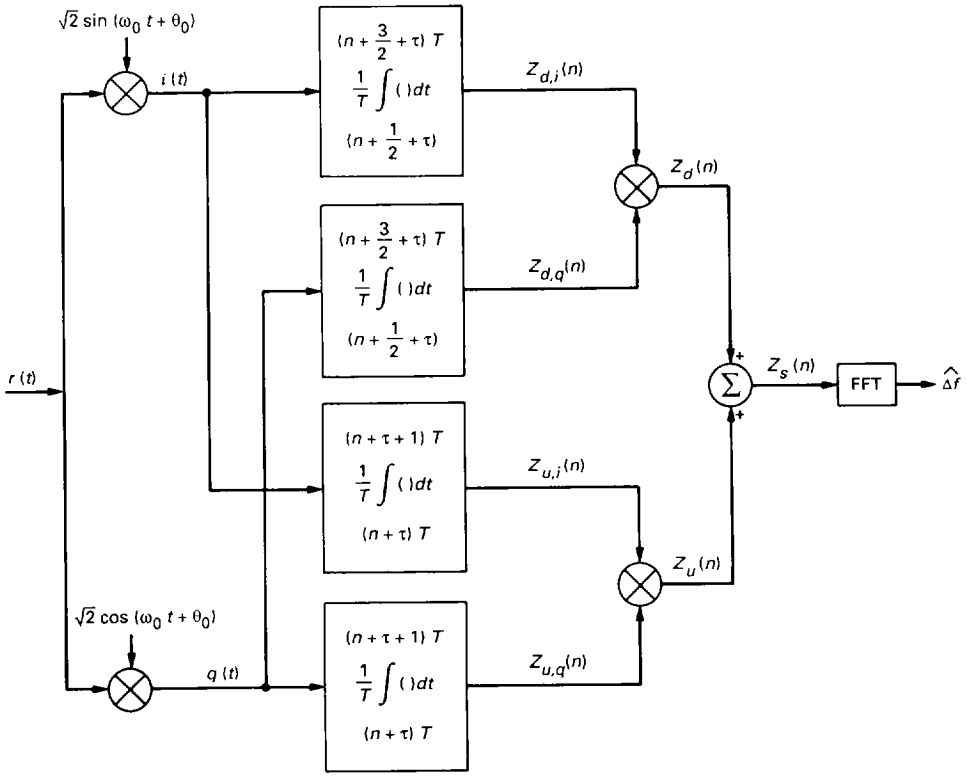

Fig. 3. Staggered-symbol integration technique.

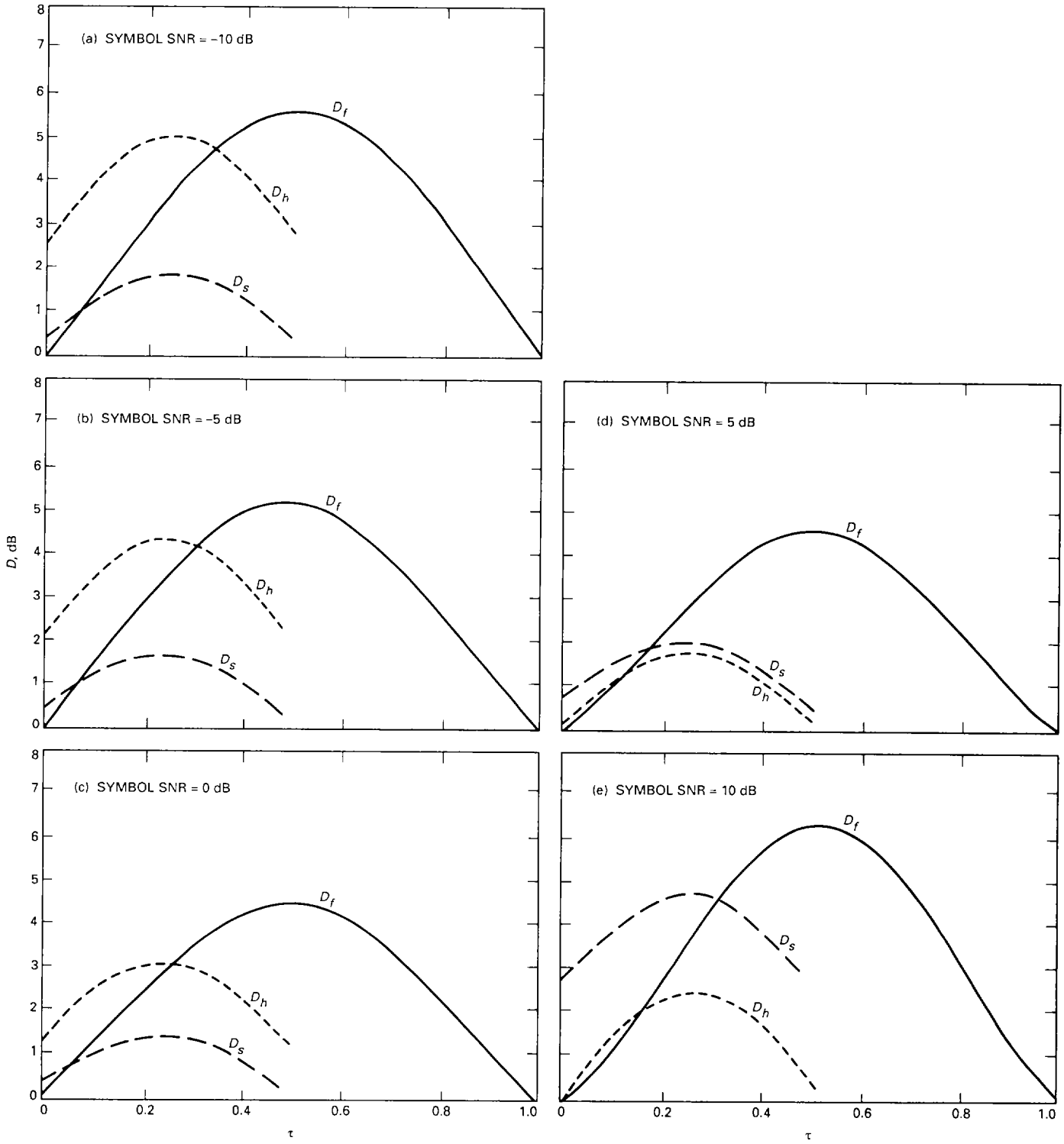

Fig. 4. Signal-to-noise degradation versus symbol timing error for various symbol SNRs.

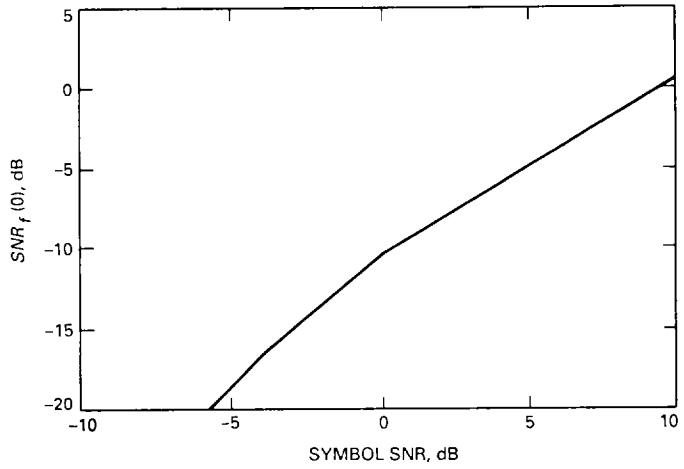

Fig. 5. $SNR_f(0)$ versus received symbol SNR.

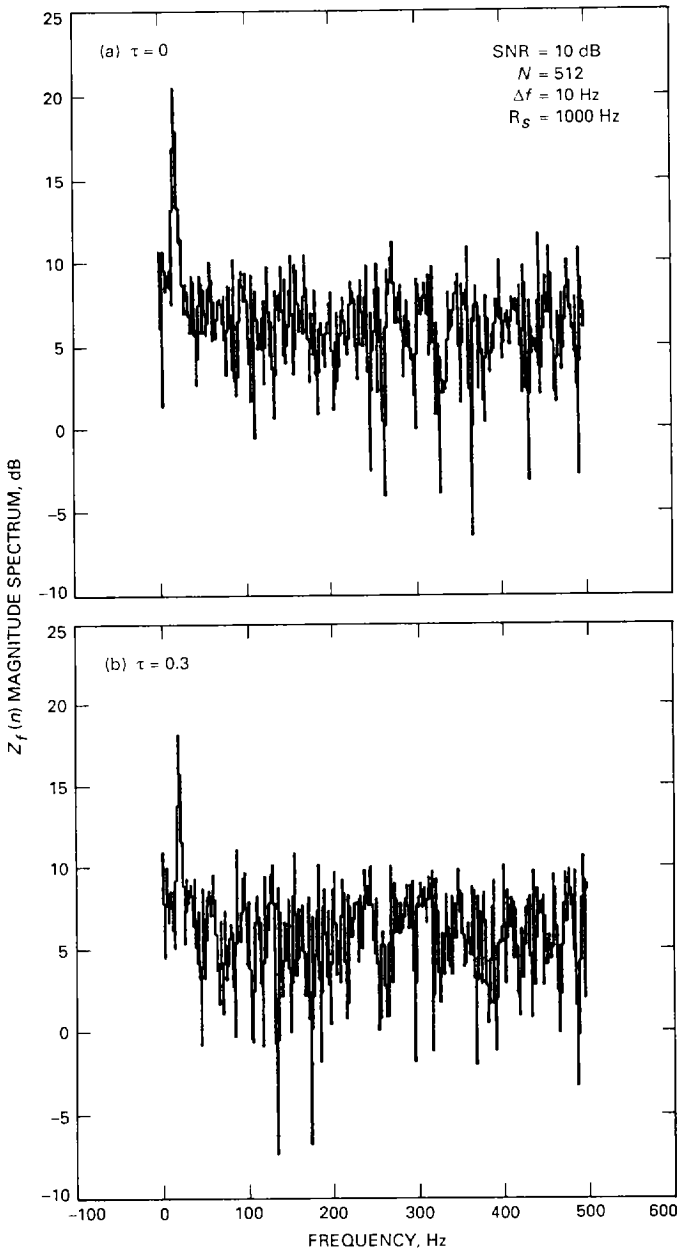

Fig. 6. Full-symbol error signal magnitude spectrum.

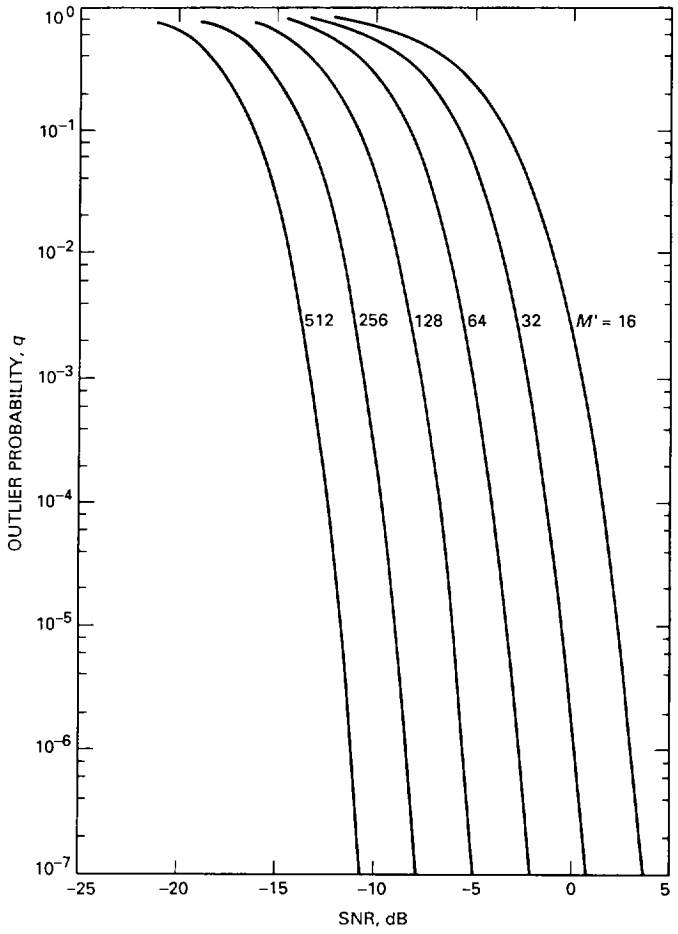

Fig. 7. Probability of outlier versus SNR.

Appendix A

Derivation of the Full-Symbol Error Signal

The full-symbol integration technique is shown in Fig. 1. As noted in Section II of the main text, $r(t)$ is the received suppressed-carrier BPSK signal downconverted to an appropiate IF frequency. Hence, it can be represented mathematically by Eqs. (1)–(3). Referring to Fig. 1, $r(t)$ is first demodulated and then integrated over a moving T-sec window to produce the sequences $Z_{f,i}(n)$ and $Z_{f,q}(n)$, as given by Eqs. (4) and (5). The noise samples $N_{f,i}(n)$ and $N_{f,q}(n)$ are given by

$$\begin{aligned} N_{f,i}(n) = &- \sin\big(\Delta\omega(nT + T/2 + \tau T) + \phi\big) \\ &\times \frac{1}{T}\int_{(n+\tau)T}^{(n+1+\tau)T} n_c(t)dt \\ &- \cos\big(\Delta\omega(nT + T/2 + \tau T) + \phi\big) \\ &\times \frac{1}{T}\int_{(n+\tau)T}^{(n+1+\tau)T} n_s(t)dt \end{aligned} \tag{A-1}$$

and

$$\begin{aligned} N_{f,q}(n) = &\cos\big(\Delta\omega(nT + T/2 + \tau T) + \phi\big) \\ &\times \frac{1}{T}\int_{(n+\tau)T}^{(n+1+\tau)T} n_c(t)dt \\ &- \sin\big(\Delta\omega(nT + T/2 + \tau T) + \phi\big) \\ &\times \frac{1}{T}\int_{(n+\tau)T}^{(n+1+\tau)T} n_s(t)dt \end{aligned} \tag{A-2}$$

and are Gaussian with zero mean and variance $\sigma^2 = N_0/2T$. The error signal $Z_f(n)$ is given by

$$Z_f(n) = Z_{f,i}(n)Z_{f,q}(n) = s_f(n) + n_f(n) \tag{A-3}$$

where the signal part of $Z_f(n)$ is defined as

$$\begin{aligned} s_f(n) &\triangleq \mathcal{E}\big[Z_f(n)/\phi\big] \\ &= A_f(P,\tau)\sin\big(2\Delta\omega nT + 2\theta_f(\phi)\big) \end{aligned} \tag{A-4}$$

where

$$A_f(P,\tau) = \frac{P}{2}(1 - 2\tau + 2\tau^2) \tag{A-5}$$

and

$$\theta_f(\phi) = \Delta\omega T\left(\tau + \frac{1}{2}\right) + \phi \tag{A-6}$$

The effective noise $n_f(n)$ can be expressed as in Eq. (10), where

$$\begin{aligned} n_{f,ss}(n) &= P(1-\tau)\tau d_n d_{n+1} \\ &\quad \times \sin\big(2\Delta\omega nT + 2\theta(\phi)\big) \end{aligned} \tag{A-7}$$

$$n_{f,sn}(n) = \sqrt{P}D_f(n)N_f(n) \tag{A-8}$$

$$n_{f,nn}(n) = N_{f,i}(n)N_{f,q}(n) \tag{A-9}$$

and $N_f(n)$ in Eq. (A-8) is defined as

$$\begin{aligned} N_f(n) \triangleq &N_{f,q}(n)\cos\big(\Delta\omega nT + \theta_f(\phi)\big) \\ &+ N_{f,i}(n)\sin(\Delta\omega nT + \theta_f(\phi)) \end{aligned} \tag{A-10}$$

Appendix B

Derivation of the Half-Symbol Error Signal

Referring to Fig. 2, the signal $Z'_h(n)$ is the product of the inphase and quadraphase integrate-and-dump outputs. Hence

$$Z'_h(n) = Z_{h,i}(n)Z_{h,q}(n) = s'_h(n) + n'_h(n) \tag{B-1}$$

where $Z_{h,i}(n)$ and $Z_{h,q}(n)$ are given by Eqs. (17) and (18), and $s'_h(n) \triangleq \mathcal{E}[Z'_h(n)/\phi]$ becomes

$$s'_h(n) = \begin{cases} \frac{P}{2}\sin\big(2\Delta\omega n(T/2) + 2\theta'_h(\phi)\big), & n \text{ even} \\ \frac{P}{2}\big((1-2\tau)^2 + 2\tau^2\big) & \\ \times \sin\big(2\Delta\omega n(T/2) + 2\theta'_h(\phi)\big), & n \text{ odd} \end{cases} \tag{B-2}$$

and

$$\theta'_h(\phi) = \Delta\omega T\left(\tau + \frac{1}{4}\right) + \phi \tag{B-3}$$

The effective noise in Eq. (B-1) is defined as

$$n'_h(n) \triangleq n'_{h,ss}(n) + n'_{h,sn}(n) + n'_{h,nn}(n) \tag{B-4}$$

where

$$n'_{h,ss}(n) = \begin{cases} 0, & n \text{ even} \\ P(1-2\tau)2\tau d_{\frac{n-1}{2}} d_{\frac{n+1}{2}} & \\ \times \sin(2\Delta\omega n(T/2) + 2\theta'(\phi)), & n \text{ odd} \end{cases} \tag{B-5}$$

$$n'_{h,sn}(n) = \begin{cases} \sqrt{P}d_{\frac{n}{2}}N_h(n), & n \text{ even} \\ \sqrt{P}\big((1-2\tau)d_{\frac{n-1}{2}} & \\ +2\tau d_{\frac{n+1}{2}}\big)N(n), & n \text{ odd} \end{cases} \tag{B-6}$$

$$n'_{h,nn}(n) = N_{h,i}(n)N_{h,q}(n) \tag{B-7}$$

where $N_h(n)$ is as defined in Eq. (A-10), with T replaced by $T/2$ and $\theta_f(\phi)$ replaced by $\theta'_h(\phi)$.

Note that the preceding signal and noise expressions depend on whether one is working with the early (even n's) or late (odd n's) half of a symbol. Summing two consecutive samples of $Z'_h(n)$ removes this dependency and simplifies the computation of the error signal statistics. Hence, using the approximations $\sin(\Delta\omega nT) \approx \Delta\omega nT$ and $\cos(\Delta\omega nT) \approx 1$ when $\Delta\omega T << 1$, one obtains

$$Z_h(n) = \frac{1}{2}\big[Z'_h(2n) + Z'_h(2n+1)\big] = s_h(n) + n_h(n) \tag{B-8}$$

and

$$\begin{aligned} s_h(n) &= \frac{1}{2}\big[s'(2n) + s'(2n+1)\big] \\ &= A_h(P,\tau)\sin\big(2\Delta\omega nT + 2\theta_h(\phi)\big) \end{aligned} \tag{B-9}$$

where

$$A_h(P,\tau) = \frac{P}{2}(1 - 2\tau + 4\tau^2) \tag{B-10}$$

$$\theta_h(\phi) = \Delta\omega T\left(\tau + \frac{1}{4}\right) + \phi + \frac{1}{2}\tan^{-1}\left(\frac{B\Delta\omega T}{1+B}\right) \tag{B-11}$$

where $B = 1 - 4\tau + 8\tau^2$. The effective noise $n_h(n)$ in Eq. (B-8) is given by Eq. (23), where

$$\begin{aligned} n_{h,ss}(n) &= \frac{1}{2}\big[n'_{h,ss}(2n) + n'_{h,ss}(2n+1)\big] \\ &= P(1-2\tau)\tau d_n d_{n+1} \\ &\quad \times \sin\big(2\Delta\omega nT + 2\theta'_h(\phi) + \Delta\omega T\big) \end{aligned} \tag{B-12}$$

$$\begin{aligned} n_{h,sn}(n) &= \frac{1}{2}\big[n'_{h,sn}(2n) + n'_{h,sn}(2n+1)\big] \\ &= \frac{\sqrt{P}}{2}\Big[d_n N_h(2n) \\ &\quad + \big((1-2\tau)d_n + 2\tau d_{n+1}\big)N_h(2n+1)\Big] \end{aligned} \tag{B-13}$$

$$n_{h,nn}(n) = \frac{1}{2}\left[n'_{h,nn}(2n) + n'_{h,nn}(2n+1)\right]$$

$$= \frac{1}{2}\left[N_{h,i}(2n)N_{h,q}(2n)\right.$$

$$\left. + N_{h,i}(2n+1)N_{h,q}(2n+1)\right] \qquad \text{(B-14)}$$

where $N_h(n)$ is defined as

$$N_h(n) \triangleq N_{h,q}(n)\cos\left(\Delta\omega nT/2 + \theta'_h(\phi)\right)$$

$$+ N_{h,i}(n)\sin\left(\Delta\omega nT/2 + \theta'_h(\phi)\right) \qquad \text{(B-15)}$$

Appendix C

Derivation of the Staggered-Symbol Error Signal

The delayed channel error signal is given by

$$Z_d(n) = Z_{d,i}(n)Z_{d,q}(n) = s_d(n) + n_d(n) \tag{C-1}$$

where the signal part of $Z_d(n)$ is defined as

$$\begin{aligned} s_d(n) &\triangleq \mathcal{E}\left[Z_d(n)/\phi\right] \\ &= A_d(P,\tau)\sin\left(2\Delta\omega nT + 2\theta_d(\phi)\right) \end{aligned} \tag{C-2}$$

where

$$A_d(P,\tau) = \frac{P}{2}\left(\frac{1}{2} + 2\tau^2\right) \tag{C-3}$$

$$\theta_d(\phi) = \Delta\omega T(\tau + 1) + \phi \tag{C-4}$$

The effective noise $n_d(n)$ in Eq. (C-1) is given by Eq. (35), where

$$\begin{aligned} n_{d,ss}(n) = {} & P\left(\frac{1}{4} - \tau^2\right)d_n d_{n+1} \\ & \times \sin\left(2\Delta\omega nT + 2\theta_d(\phi)\right) \end{aligned} \tag{C-5}$$

$$n_{d,sn}(n) = \sqrt{P}D_{n,d}N_d(n) \tag{C-6}$$

$$n_{d,nn}(n) = N_{d,i}(n)N_{d,q}(n) \tag{C-7}$$

and

$$\begin{aligned} N_d(n) = {} & N_{d,q}(n)\cos\left(\Delta\omega nT + \theta_d(\phi)\right) \\ & + N_{d,q}(n)\sin\left(\Delta\omega nT + \theta_d(\phi)\right) \end{aligned} \tag{C-8}$$

Except for the subscripts u and f, the undelayed channel error signal $Z_u(n)$ in Fig. 3 is the same as the full symbol error signal $Z_f(n)$ derived in Appendix A, and given by Eqs. (A-3) through (A-10). Hence, the staggered-symbol error signal $Z_s(n)$, which is the sum of the delayed and undelayed error signals, is given by

$$Z_s(n) = Z_d(n) + Z_u(n) = s_s(n) + n_s(n) \tag{C-9}$$

and

$$\begin{aligned} s_s(n) &= s_d(n) + s_u(n) \\ &= A_s(P,\tau)\sin\left(2\Delta\omega nT + 2\theta_s(\phi)\right) \end{aligned} \tag{C-10}$$

where

$$A_s(P,\tau) = \frac{P}{2}\left(\frac{3}{2} - 2\tau + 4\tau^2\right) \tag{C-11}$$

$$\theta_s(\phi) = \Delta\omega T\left(\tau + \frac{1}{2}\right) + \phi + \frac{1}{2}\tan^{-1}\left(\frac{A_u\Delta\omega T}{A_u + A_d}\right) \tag{C-12}$$

The amplitudes A_u and A_d are given by Eqs. (A-5) and (C-3), and the effective noise $n_s(n)$ can be expressed as

$$\begin{aligned} n_s(n) &= n_u(n) + n_d(n) \\ &\triangleq n_{s,ss}(n) + n_{s,sn}(n) + n_{s,nn}(n) \end{aligned} \tag{C-13}$$

where

$$\begin{aligned} n_{s,ss}(n) &= n_{d,ss}(n) + n_{u,ss}(n) \\ &= P\left(\frac{1}{4} + \tau - 2\tau^2\right)d_n d_{n+1} \\ &\quad \times \sin\left(2\Delta\omega nT + 2\theta'_s(\phi)\right) \end{aligned} \tag{C-14}$$

$$\begin{aligned} n_{s,sn}(n) &= n_{d,sn}(n) + n_{u,sn}(n) \\ &= \sqrt{P}\left[D_d(n)N_d(n)\right. \\ &\quad \left. + D_u(n)N_u(n)\right] \end{aligned} \tag{C-15}$$

$$n_{s,nn}(n) = n_{d,nn}(n) + n_{u,nn}(n)$$

$$= N_{d,i}(n)N_{d,q}(n) + N_{u,i}(n)N_{d,q}(n) \tag{C-16}$$

The phase $\theta'_s(\phi)$ in Eq. (C-14) is given by

$$\theta'_s(\phi) = \Delta\omega T\left(\tau + \frac{1}{2}\right) + \phi + \frac{1}{2}\tan^{-1}\left(\frac{B_1\Delta\omega T}{B_2 + B_1}\right) \tag{C-17}$$

where $B_1 = 0.25 - \tau^2$ and $B_2 = (1-\tau)\tau$, and the noises $N_d(n)$ and $N_u(n)$ are given by Eqs. (C-8) and (A-10).

Unlike the previous two techniques, the noises due to the signal–noise product and noise–noise product for this technique are nonwhite, with auto-correlation given by

$$R_{sn}(n) = P(2 - 3\tau + 6\tau^2)\sigma^2\delta(n)$$

$$+ P\left(\frac{1}{2} + \frac{1}{2}\tau - \tau^2\right)\big(\delta(n-1) + \delta(n+1)\big) \tag{C-18}$$

$$R_{nn}(n) = \frac{5}{2}\sigma^4\delta(n) + \frac{1}{4}\sigma^4\big(\delta(n-1) + \delta(n+1)\big) \tag{C-19}$$

From the last two equations, the average power of $n_{s,sn}$ and $n_{s,nn}$ is given as

$$\sigma^2_{s,sn} = P(2 - 3\tau + 6\tau^2)\sigma^2 \tag{C-20}$$

$$\sigma^2_{s,nn} = \frac{5}{2}\sigma^4 \tag{C-21}$$

Appendix D

Detection Probability of a Tone in White Noise

This appendix briefly rederives the results of [3] which apply to this article. Suppose

$$x(i) = A\sin(2\pi f i T_s + \theta) + n(i) \qquad \text{(D-1)}$$

where $f_s = 1/T_s$ is the rate at which the continuous process $x(t)$ was sampled, and the $n(i)$'s represent independent Gaussian random variables with zero mean and variance σ^2. Let $X(k)$ be the M-point discrete Fourier transform of $x(i)$. That is,

$$X(k) = \frac{1}{M}\sum_{i=0}^{M-1} x(i)\exp\left(-\frac{j2\pi ik}{M}\right), \quad k = 0, 1, ..., M-1 \qquad \text{(D-2)}$$

Since $x(i)$ is real, there are $M/2+1$ distinct cells of the M total cells. Then, upon observing the $M/2+1$ distinct cells of the magnitude spectrum of $X(k)$, the probability of detecting the real tone is given by [3] to be

$$p = \int_0^\infty 2M'(SNR)ye^{-M'(SNR)(y^2+1)} \times I_0[2M'y(SNR)] \times [1 - y^2e^{-M'(SNR)}]^{M'}dy \qquad \text{(D-3)}$$

where $M' = M/2$ and where $SNR \triangleq \frac{A^2}{2\sigma^2}$, and where $I_0(\cdot)$ is the modified Bessel function of the first kind.

The outlier probability $q = 1 - p$ is shown in Fig. 7 as a function of SNR. Further note that Fig. 7 is slightly different than the one presented in [3], because this article considers real FFTs whereas [3] applies to complex FFTs.